

2.3 Precision Electroweak Program

2.3.1 Introduction

The comparison of diverse precision experimental measurements to expectations from the Standard Model [1] allows precise tests sensitive to new physics at scales above the electroweak scale, as well as a determination of the Higgs mass within the framework of the model [2]. Global electroweak fits until now have been largely dominated by LEP data, with contributions from the SLAC polarization measurement, W mass measurements in $\bar{p}p$ interactions, neutrino neutral current data, and most recently the measurement of the top mass [3] at the Tevatron.

Precision measurement of the top mass and the W mass are primary goals of CDF II. In addition, in the electroweak sector, the W width and leptonic branching ratio, the tri-linear couplings of the W , Z and γ , and the forward-backward charge asymmetry of dileptons at the Z pole and above are important Standard Model parameters. These measurements together will take the global electroweak fit to a new level of precision, and do so completely in the context of a single experiment.

In this section we discuss measurements directly involving the gauge bosons. We begin with the expected event yields of W , Z , and diboson production for Run II with 2 fb^{-1} . We then discuss the CDF Electroweak measurements for Run I and CDF II prospects for Run II.

Studies of the Run II sensitivities for Electroweak physics at CDF II, and their competitiveness with LEP-II, LHC and NLC experiments are also detailed in the DPF Summary Report of the Working Subgroup on Anomalous Gauge Boson Interactions [4] and more recently in the Intermediate Vector Boson Physics chapter of the TeV-2000 Report [5].

2.3.2 Event Yields

The Electroweak physics potential can best be illustrated by the expected event yields for W , Z , and diboson production. We first list the event yields with 2 fb^{-1} with the Run Ib configuration, and compare the lepton identification and acceptances for Run Ib with those for Run II. There is a significant improvement in the event yields of W , Z , and diboson production when the lepton and photon acceptances are

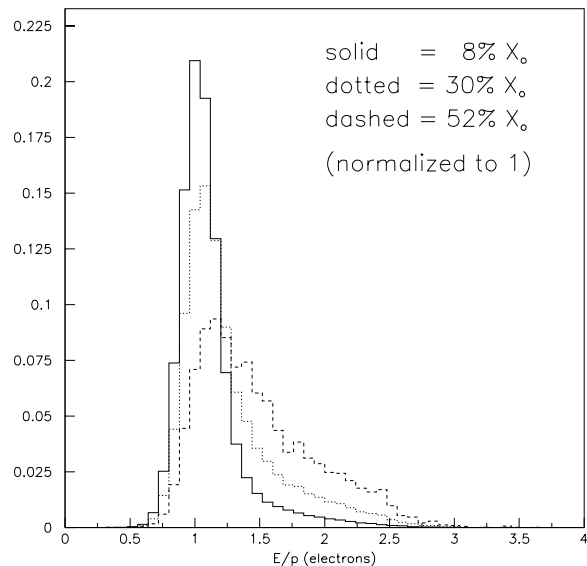


Figure 2.9: E/p distribution of electrons from W decays. The solid (dotted, dashed) histogram uses 8% X_o (17% X_o , 30% X_o) of the detector material up to the middle of the CTC.

extended to high η , and the high η leptons and photons also enable some previously inaccessible physics.

2.3.2.1 Improvement from the integrated luminosity and \sqrt{s}

The expected event yields for W , Z , and diboson production, when the Run Ib configuration is assumed, are listed in Table 2.4. The results are based on the acceptances and efficiencies measured from Run I analyses. For Run II, \sqrt{s} will be 2.0 TeV instead of 1.8 TeV, which will increase W and Z cross sections by $\sim 12\%$ and diboson cross sections by $13\% \sim 22\%$.

2.3.2.2 Lepton Identification and Acceptances

We compare the lepton identification and acceptances for Run I with those for Run II.

• Electrons

The identification of electrons relies heavily on the correlation of tracking information with calorimetric measurement of shower energy and position.

For Run II, the identification and treatment of central electrons will be very reminiscent of Run

channel		number of events	$\sigma_{2.0\text{TeV}}/\sigma_{1.8\text{TeV}}$
		$\sqrt{s} = 1.8 \text{ TeV}, (A, \epsilon)^{\text{RunIb}}$	
$W \rightarrow e\nu$	(e^c)	1,000,000	1.12
$W \rightarrow e\nu$	(e^p)	400,000	1.12
$W \rightarrow \mu\nu$	(μ^c)	600,000	1.12
$W \rightarrow \mu\nu$	(μ^f)	44,000	1.12
$Z \rightarrow ee$	$(e^c, e^{c,p,f})$	130,000	1.12
$Z \rightarrow \mu\mu$	(μ^c, μ^c)	50,000	1.12
$W\gamma, E_T^\gamma > 10 \text{ GeV}$	$(\gamma^{c,p})$	1,500	1.13
$Z\gamma, E_T^\gamma > 10 \text{ GeV}$	$(\gamma^{c,p})$	450	1.13
$WW \rightarrow \ell\nu\ell\nu$		77	1.17
$WZ \rightarrow \ell\nu\ell\ell$		9.6	1.22
$ZZ \rightarrow \ell\ell\ell\ell$		1.2	1.19

Table 2.4: Expected W , Z , and diboson event yields with 2 fb^{-1} when the Run Ib configuration is assumed, and the increase in cross sections with $\sqrt{s} = 2.0 \text{ TeV}$. c , p , and f for electrons represent Run I CEM, PEM, and FEM, and c and f for muons represent Run I CMU/P and FMU.

channel	lepton (e) rapidity			
	1.0	1.5	2.0	2.5
$W \rightarrow \ell\nu$	(1.00)	1.42	1.98	2.26
$Z \rightarrow \ell\ell$	(1.00)	2.13	3.30	3.61
$W\gamma, E_T^\gamma > 10 \text{ GeV}, \eta^\gamma < 1.0$	(1.00)	1.26	1.48	1.53
$W\gamma, E_T^\gamma > 10 \text{ GeV}, \eta^\gamma < 1.5$	1.28	1.64	1.95	2.03
$W\gamma, E_T^\gamma > 10 \text{ GeV}, \eta^\gamma < 2.0$	1.54	2.01	2.42	2.53
$W\gamma, E_T^\gamma > 10 \text{ GeV}, \eta^\gamma < 2.5$	1.63	2.14	2.59	2.72
$Z\gamma, E_T^\gamma > 10 \text{ GeV}, \eta^\gamma < 1.0$	(1.00)	1.68	2.26	2.36
$Z\gamma, E_T^\gamma > 10 \text{ GeV}, \eta^\gamma < 1.5$	1.27	2.17	2.96	3.11
$Z\gamma, E_T^\gamma > 10 \text{ GeV}, \eta^\gamma < 2.0$	1.51	2.63	3.65	3.85
$Z\gamma, E_T^\gamma > 10 \text{ GeV}, \eta^\gamma < 2.5$	1.59	2.79	3.92	4.15
$WW \rightarrow \ell\nu\ell\nu$	(1.00)	1.70	2.14	2.33
$WZ \rightarrow \ell\nu\ell\ell$	(1.00)	2.68	4.37	5.33
$ZZ \rightarrow \ell\ell\ell\ell$	(1.00)	2.62	4.10	4.81

Table 2.5: Improvement in acceptances of W , Z , and diboson production for various lepton and photon η cuts, normalized to those with η of leptons and photons less than 1 (listed in parentheses), by using Monte Carlo events simulated on the basis of the Run I detector and triggers. The entries below are for the electron channel only, and the muon channel results will be very similar to the electron ones. Electrons are required to have $E_T > 25 \text{ GeV}$.

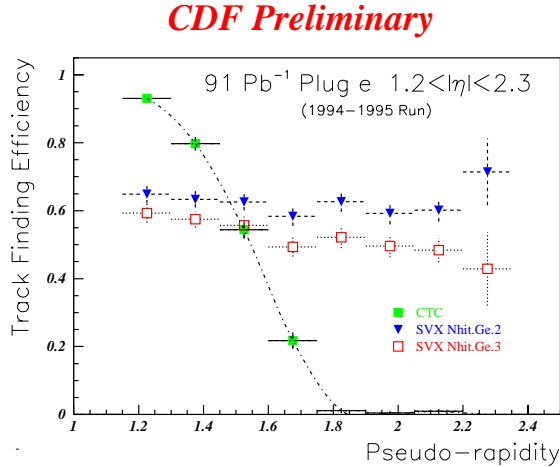


Figure 2.10: The $|\eta_{\text{det}}|$ distributions of plug W electrons. Events in CTC sample are concentrated in the low $|\eta_{\text{det}}|$ because the CTC track finding efficiency quickly falls. The SVX sample events are populated more uniformly in $|\eta_{\text{det}}|$.

I: the EM calorimeter is identical, and the tracking performance and amount of material traversed will be very similar.

The interesting new feature for Run II will be the identification of electrons in the plug region $1.0 \leq |\eta| \leq 2.0$. For Run I, the purity of the plug electrons was relatively poor mainly because the tracking information in this region was poor or completely absent. The CTC track-finding efficiency fell very rapidly in the range of detector η (η_{det}) covered by the plug calorimeter. As shown in Figure 2.10, it is about 60% at $|\eta_{\text{det}}| \sim 1.5$ and almost 0 at $|\eta_{\text{det}}| \sim 1.8$.

Recently a new technique for the charge determination was developed where the SVX track is used in conjunction with the plug electromagnetic cluster (see Section 2.3.7). With this technique, the electron charge can be determined up to $|\eta_{\text{det}}| \sim 2.3$. The efficiency of this technique at present is only 50 – 60 % due to the short length of the SVX'.

With SVX II+ISL+COT integrated tracking for Run II, the momentum information will be better, more efficient, and available over a wider

range in η . The total material before electrons hit the plug upgrade detector will be roughly 50-60wide E/p distribution as shown in Figure 2.9, but overall we will improve the electron efficiency quite a bit, reduce QCD background, and make the QCD background estimate easier. Plug electrons will significantly improve the yields for W and Z bosons, and allow us to examine some previously inaccessible electroweak physics topics at high η .

As listed in Table 2.5, the acceptances of W and Z production are almost doubled by changing the η cut from $|\eta| < 1$ to $|\eta| < 2$. The acceptances of the diboson productions are almost tripled (see Table 2.5 and Figures 2.11 and 2.12). More importantly, the high η leptons and photons provide opportunities for previously inaccessible physics. The high η leptons are very sensitive to physics in the small x region (the W charge asymmetry and Drell-Yan cross sections; see Section 2.3.7), and the high η leptons and photons are essential to observe the radiation zero in the $W\gamma$ production (see Section 2.3.5).

Therefore it is important to trigger on plug electrons. The expected Level-1 and Level-3 trigger rates for the plug electrons are much smaller than the available bandwidth, but Level-2 is an issue. Extrapolating from Run Ib Level-2 plug electron trigger rates, the Run II plug electron rate in the region $1.1 < |\eta_{\text{det}}| < 2.4$ using the simple requirement $E_T^{\text{PEM}} > 20\text{GeV}$ is estimated to be about 40 Hz at $\mathcal{L} = 2 \times 10^{32}$ and the 132 ns bunch spacing. This trigger was not efficient enough for W events for Run I. The more efficient trigger was $E_T^{\text{PEM}} > 15\text{GeV}$ and $\cancel{E}_T > 15\text{GeV}$. At $\mathcal{L} = 2 \times 10^{32}$ and the 132 ns bunch spacing, the rate of this trigger is estimated to be about 70 Hz. For the trigger system designed to handle 300 Hz at Level 2, this is uncomfortably high. Therefore it is essential to improve the background rejection by providing additional detector information to the Level-2 system. For example, the Plug shower maximum detector information, the isolation requirement, or the high η track requirement can improve the rejection.

- **Central muons**

The central muon quality won't change much from Run I to Run II. The Run II tracking de-

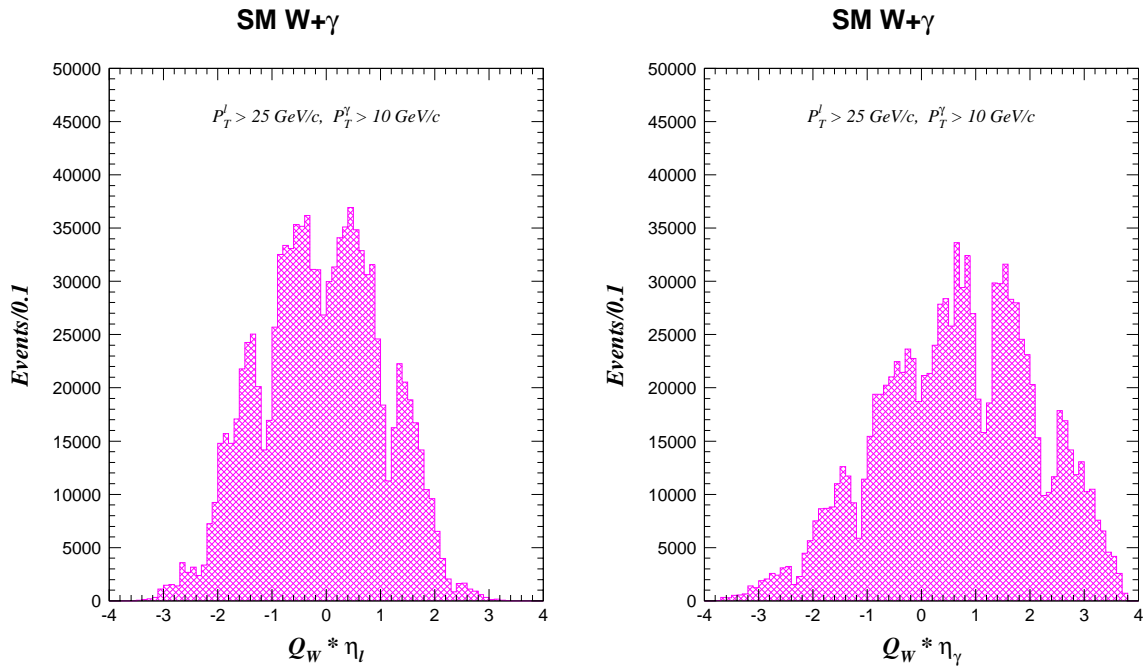


Figure 2.11: The lepton charge signed pseudo-rapidity distribution of the lepton and the photon in the $W\gamma$ production.

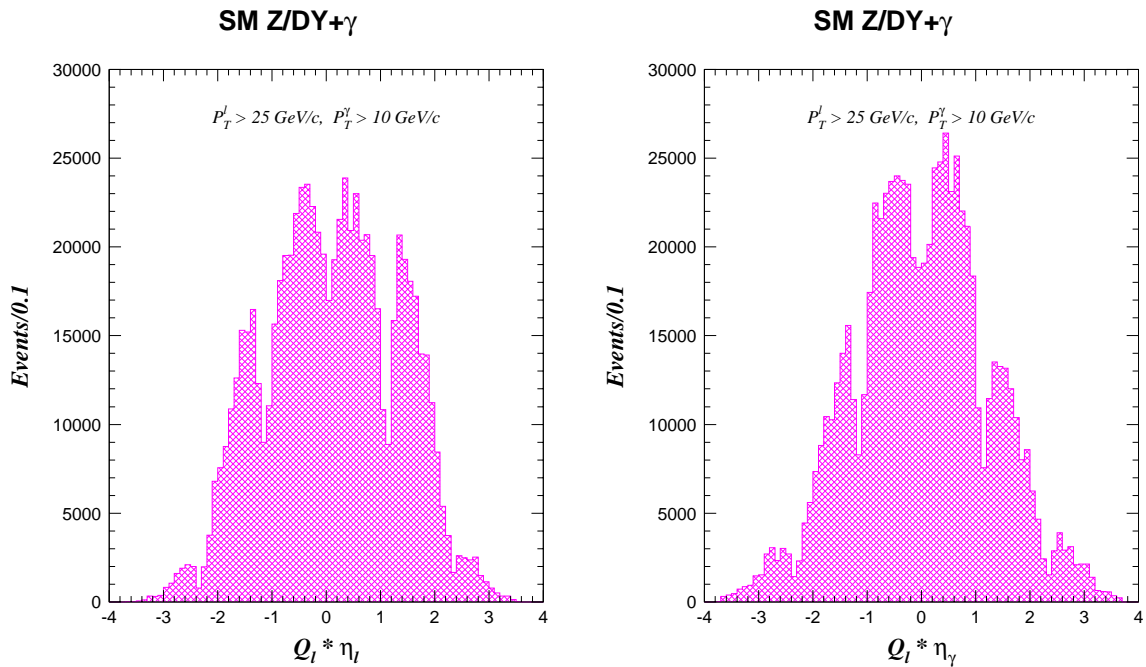


Figure 2.12: The lepton charge signed pseudo-rapidity distribution of the lepton and the photon in $Z\gamma$ production.

tectors will be able to maintain the good resolution and efficiency despite the higher luminosity. There will be additional muon acceptance for Run II, and the samples of $W \rightarrow \mu\nu$ and $Z \rightarrow \mu\mu$ will both be increased by 30%.

- **Intermediate muons** As described in Sec 10.6, muon detection will be added in the region $1.0 \leq |\eta| \leq 2.0$. The arguments for intermediate muons are similar to those for plug electrons: they will be quite helpful for multilepton signatures such as WW , WZ , ZZ decaying to leptons, and for the W charge asymmetry measurement. These will also provide a good handle to reduce the $Z \rightarrow \mu\mu$ background in the $W \rightarrow \mu\nu$ sample.

2.3.3 W Mass

The mass of the W boson is a fundamental parameter of the Standard Model. A direct measurement of M_W can be compared with the prediction from LEP and SLC results as a test of the SM. In the context of other precise electroweak measurements, direct and precise measurements of M_W and M_{top} provide an indirect constraint on the Higgs boson mass, M_H , via electroweak radiative corrections. The ultimate test of the SM may lie in the comparison of this indirect determination of M_H with its direct observation.

At the Tevatron, the W mass is extracted from a fit to the W transverse mass, M_T^W , distribution which sharply peaks in the vicinity of M_W . The 4 pb⁻¹ of the 1988-89 Tevatron Collider run enabled CDF to measure the W mass to be

$$M_W = 79.91 \pm 0.39 \text{ GeV}/c^2 \text{ [7]},$$

and with 19 pb⁻¹ from Run Ia CDF measured

$$M_W = 80.41 \pm 0.18 \text{ GeV}/c^2 \text{ [8]}.$$

This measurement is an important component of the world average of $M_W = 80.35 \pm 0.13 \text{ GeV}$. The uncertainties for the Run Ia measurement are shown in Table 2.6. Figure 2.13 (a) shows the sensitivity in the M_W - M_{top} plane of this result when combined with the value $M_{\text{top}} = 176.8 \pm 6.5 \text{ GeV}/c^2$, compared to theoretical predictions based on electroweak radiative corrections [9].

In the following section we will argue that a data set of 2 fb⁻¹ will allow CDF II to measure the W mass to $\pm 40 \text{ MeV}/c^2$, which is comparable to the overall

LEP2 expectation ($\sim 40 \text{ MeV}$). Figure 2.13 (b) shows the sensitivity in the M_W - M_{top} plane of this estimate when combined with the expected precision δM_{top} for the same dataset. The precision measurement of the W boson and top quark mass with CDF II will allow inference of the Standard Model Higgs boson mass with an uncertainty of less than $\delta M_H \sim 2 M_H$ [2].

The uncertainties in the current Run Ib measurement scale rather well with statistics from the previous measurement; while the difficulty of the measurement has increased, no systematic limitation is yet evident. The statistical improvement using $\sim 90 \text{ pb}^{-1}$ of data from Run Ib is illustrated in Figure 2.14. For Run II, statistical uncertainty and most of systematic uncertainties are expected to be reduced significantly. The individual uncertainties are briefly discussed.

- **Statistical uncertainty**

For Run Ib the typical instantaneous luminosity at the beginning of runs was about $2 \times 10^{31} \text{ cm}^{-2} \text{ sec}^{-1}$ and we had about 2.5 extra minimum bias events overlying W and Z events on average. This results in about a 10% loss in statistical precision due to the degraded resolution in the recoil measurement in Run Ib as opposed to Run Ia. For 132 ns operation in Run II the increased number of bunches will more than compensate for the higher luminosity and the number of extra minimum bias events will be to the Run Ia level. This will give us a situation which is better than Run Ib.

- **Track momentum scale and resolution**

Scale: Knowledge of material in the tracking volume is of importance in determining the momentum and energy scale. The associated systematics are the uncertainties in the muon energy loss (dE/dx) for the momentum scale and in the radiative shift of the electron E/p peak for the energy scale. Although the amount of material in the tracking volume will be changed we have shown that photon conversions allow us to measure the amount of material in radiation length quite accurately, as illustrated in Figure 2.15 and can reduce the uncertainties on the W mass measurement. However, the dE/dx muon energy loss requires information of the material type in addition to the radiation length. For example, unknown type of 1% X₀ material leads to about 10 MeV uncertainty in the W

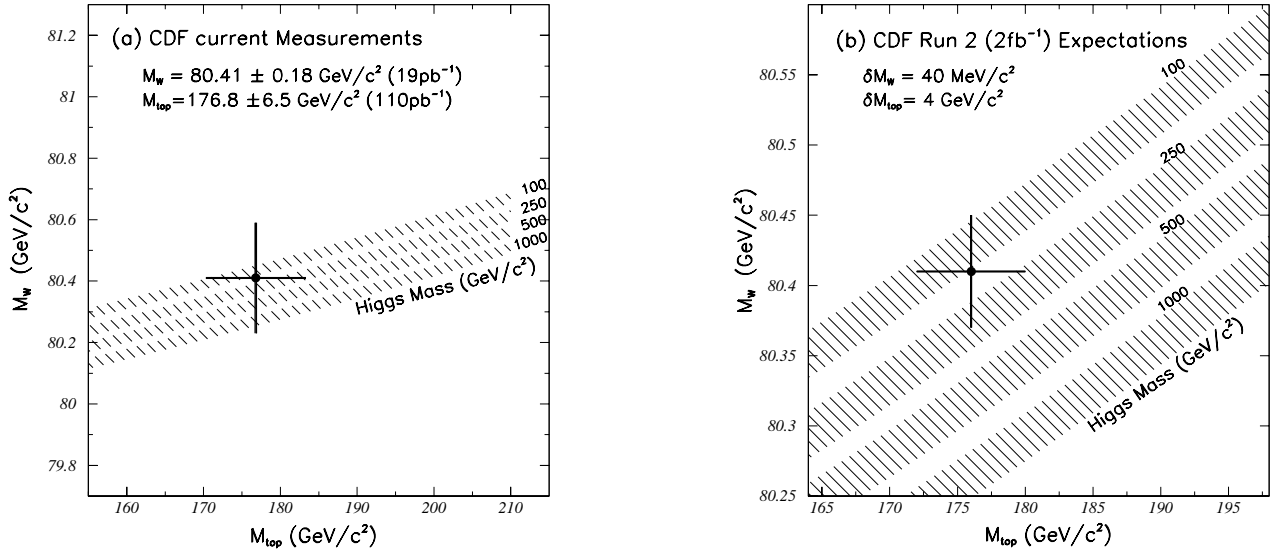


Figure 2.13: The data point in the left figure represents the CDF measurements of M_W and M_{top} , and the point in the right figure represents the CDF II estimate for 2 fb^{-1} . The curves are from a calculation [9] of the dependence of M_W on M_{top} in the minimal standard model using several Higgs masses. The bands are the uncertainties obtained by folding in quadrature uncertainties on $\alpha(M_Z^2)$, M_Z , and $\alpha_s(M_Z^2)$.

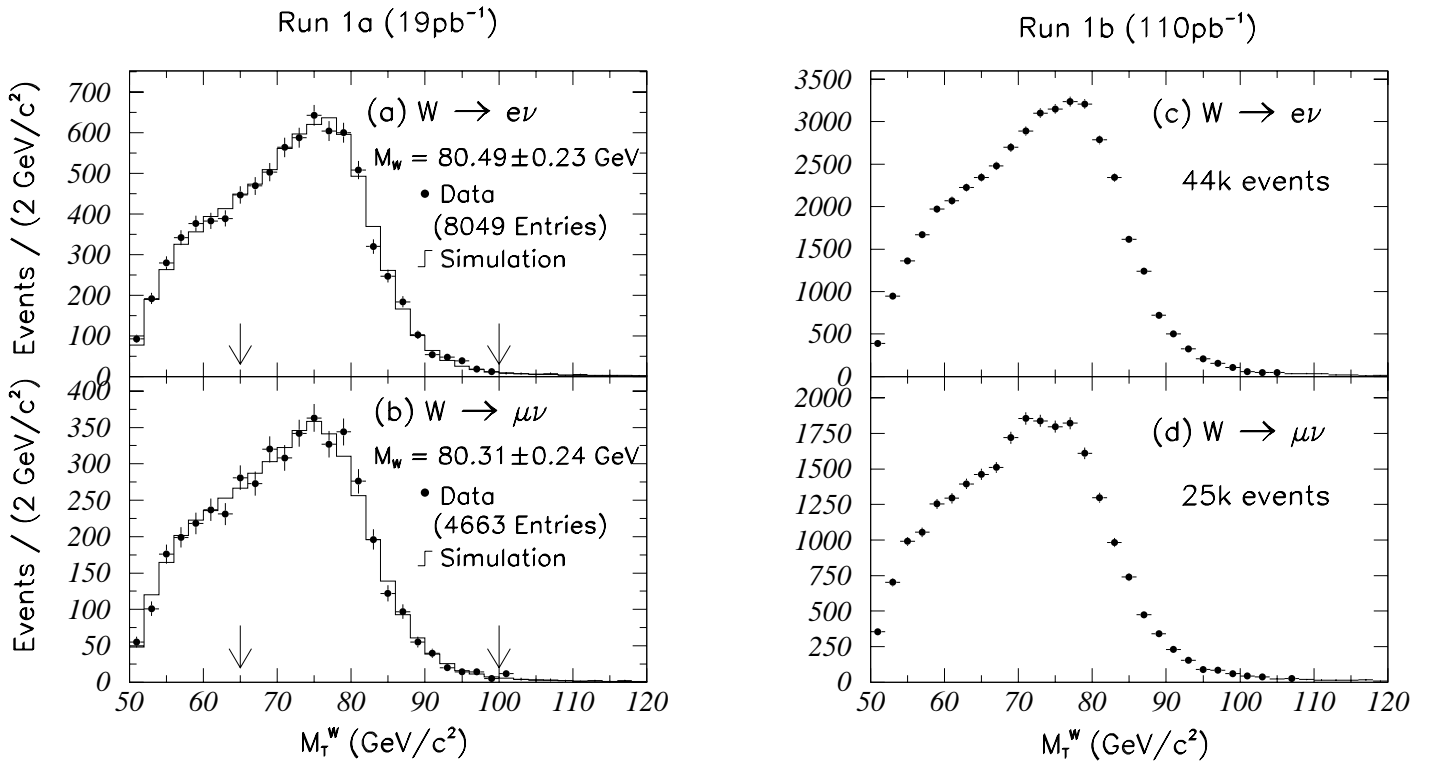


Figure 2.14: Transverse mass distributions for $W \rightarrow e\nu$ and $W \rightarrow \mu\nu$ from Run Ia (a and b) which gave a $\pm 180 \text{ MeV}/c^2$ measurement of the W mass, and the equivalent preliminary distributions from the first 67 pb^{-1} of Run Ib (c and d).

Source of Uncertainty	Uncertainty (MeV/c ²)		
	$W \rightarrow e\nu$	$W \rightarrow \mu\nu$	Common
Statistical	145	205	–
Lepton Energy/Momentum Scale	120	50	50
Lepton Energy/Momentum Resolution	80	60	–
Recoil modeling	60	60	60
Trigger, Event Selection	25	25	–
Backgrounds	10	25	–
W Production Model (P_T^W , PDF, QCD higher order corr., QED rad. corr.)	75	75	65
Fitting	10	10	–
Total Uncertainty	230	240	100
e and μ Combined Uncertainty	180		

Table 2.6: Summary of uncertainties in the Run Ia W mass measurement.

Source of Uncertainty	Uncertainty (MeV/c ²)		
	$W \rightarrow e\nu$	$W \rightarrow \mu\nu$	Common
Statistical	14	20	–
Lepton Energy/Momentum Scale	20	15	15
Lepton Energy/Momentum Resolution	8	6	–
Recoil modeling	6	6	6
Trigger, Event Selection	10	10	–
Backgrounds	5	10	–
W Production Model (P_T^W , PDF, QCD higher order corr., QED rad. corr.)	30	30	30
Fitting	5	5	–
Total Uncertainty	42	40	34
e and μ Combined Uncertainty	38		

Table 2.7: Estimate of uncertainties in the W mass measurement for 2 fb⁻¹.

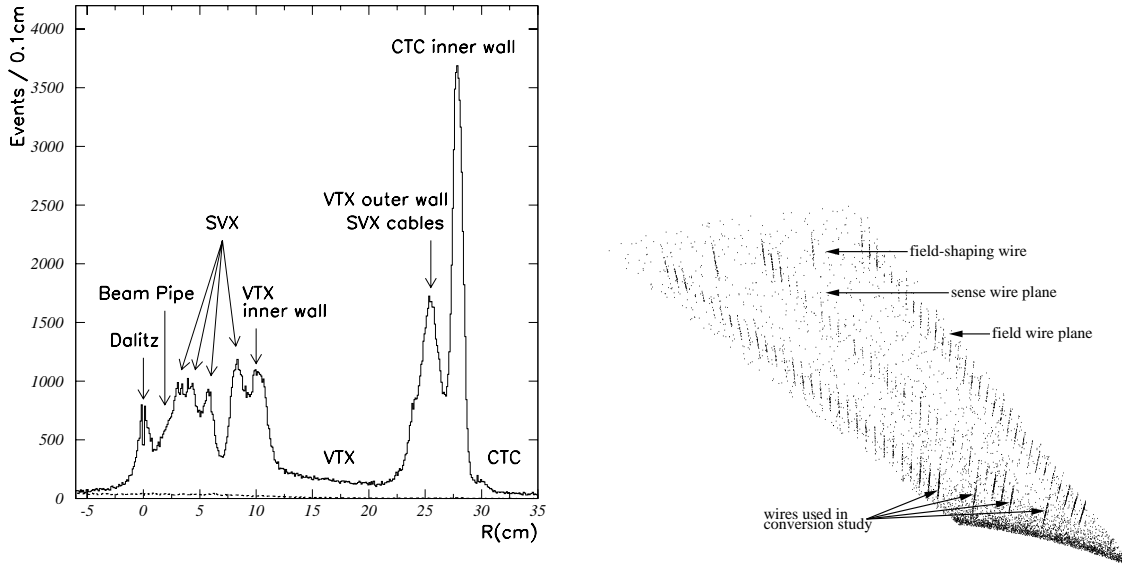


Figure 2.15: Left: The radial distributions for conversions (solid line) and background (dashed line). Right: Reconstructed photon conversion vertex density in the r - ϕ plane for the innermost super-layer in the CTC, folded into $1/30$ of the circumference (this layer has 30-fold symmetry).

mass measurement.

Resolution: It is important to assess the impact of high luminosity running on the track momentum resolution. In Run Ib, the CTC track resolution degraded with luminosity, but could be recovered when SVX hits or the SVX beam position were added to the tracking. For instance, if we compare early Run Ib ($\mathcal{L} \sim 0.2 \times 10^{31}$) to later Run Ib ($\mathcal{L} \sim 1 \times 10^{31}$), the CTC track resolution observed in the width of the J/ψ peak worsens by 35%, but the SVX + CTC track resolution worsens by only 10%. The new tracking system incorporates this linking naturally across all detectors (for $|\eta| \leq 1.0$), and as a consequence, the momentum resolution at $N = 6$ ($\mathcal{L} = 2 \times 10^{32} \text{cm}^{-2}\text{s}^{-1}$) is almost identical to the resolution at $N = 1$. This is discussed in detail in Chapter 7, see especially Sec. 7.6.3 and Fig. 7.14.

The M_W uncertainty due to the momentum resolution uncertainty will scale with statistics since the resolution is determined using $Z \rightarrow \mu\mu$ events.

- **Calorimeter energy scale and resolution**

The dominant uncertainty in the electron en-

ergy scale for Run Ia was from the uncertainty in amount of material in radiation length, and statistics. As described above, the amount of material is expected to be well measured by photon conversion events for Run II, but with complications due to the increase in the amount of material: the statistics of the conversion sample will be reduced by $\sim 13\%$ (because of the broadening of the electron E/p), and higher order QED corrections might be necessary.

The M_W uncertainty due to the energy resolution uncertainty will scale with statistics since the resolution is determined using $Z \rightarrow ee$ events.

- **Recoiling energy modeling**

The detector response to the recoil energy against W is directly calibrated using $Z \rightarrow ee$. Therefore the uncertainty will scale with statistics. For Run II with the muon coverage at high η , $Z \rightarrow \mu\mu$ can also be used.

- **W Production model**

\underline{P}_T^W : For the P_T^W spectrum, the P_T^Z distribution from $ee, \mu\mu$ and a new theoretical calculation which includes soft gluon resummation effects

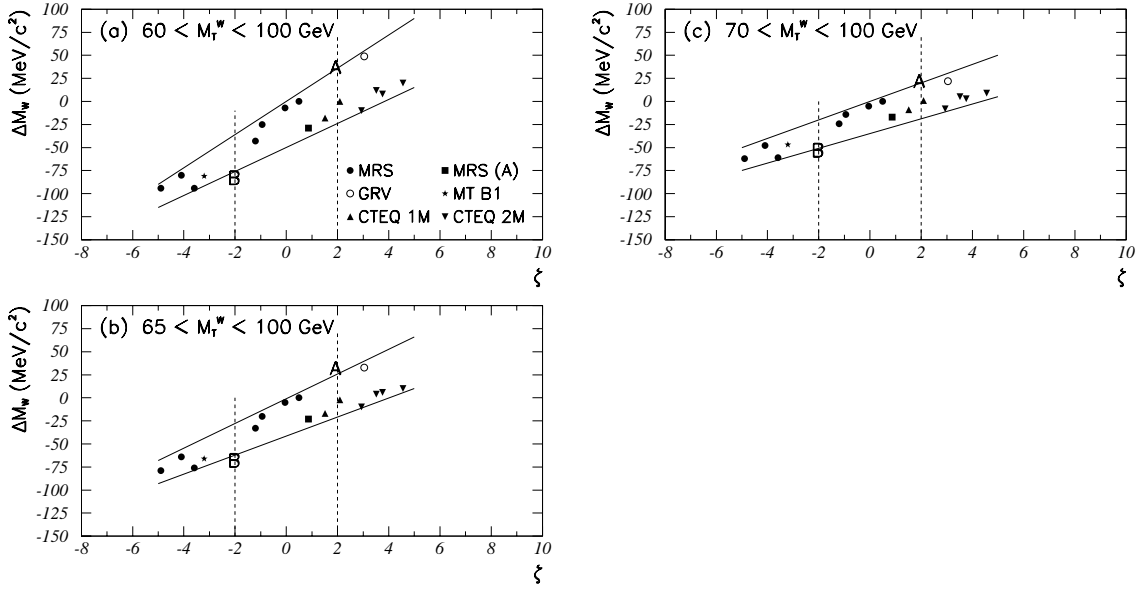


Figure 2.16: Change in derived $W \rightarrow e\nu$ mass (ΔM_W^e) versus the signed deviation in units of standard deviations from the average Run Ia W asymmetry measurement (ζ) for various PDFs. The lower edge of the fitting region is (a) 60, (b) 65, and (c) 70 GeV. Note that raising the lower edge of the fitting region makes the result less sensitive to PDFs, particularly for variation not correlated to the asymmetry.

and W , Z decays are expected to provide appropriate checks and improved theoretical guidance, and will make it possible to reduce the current uncertainty of 45 MeV in M_W substantially.

Parton Distribution Functions: The Run Ia uncertainty in PDF's (50 MeV) was constrained by the CDF W asymmetry measurement (see Figure 2.16; the dotted lines indicate ± 2 standard deviations from the Run Ia W asymmetry measurement.) This particular advantage in constraining the PDF systematic uncertainty in the W mass may soon be saturated, and with the same technique the uncertainty of 25 MeV in M_W is estimated for Run II. (With more statistics, the dotted lines in Figure 2.16 will get closer to zero, but ΔM_W won't.) This will then be the dominant uncertainty in M_W for Run II.

The fact that the PDF uncertainty in M_W does not scale with the W asymmetry uncertainty indicates that parameters in PDFs sensitive to the W charge asymmetry are not the only ones sensitive to the M_T^W distribution. Monte Carlo studies show that the W charge asymmetry is sensi-

tive to $\langle u \rangle$ and $\langle d \rangle$, and the M_T^W distribution has a weak but not small dependence on σ_u^{RMS} and σ_d^{RMS} in addition to a strong dependence on $\langle u \rangle$ and $\langle d \rangle$. The y distributions of Z (y_Z) from dileptons have some sensitivity to constrain PDFs in σ_u^{RMS} and σ_d^{RMS} , and this may help reducing the PDF uncertainty in M_W . However, to do this a precise measurement (better than 1%) of Z efficiency as a function y_Z in a wide rapidity region is required.

An alternative solution to reduce the PDF uncertainty will be raising the minimum M_T^W for fitting. This is illustrated in Figure 2.16 (a), (b) and (c). However, this will imply a larger statistical uncertainty.

QCD higher order corrections : The effects of higher-order QCD corrections on the W polarization and on a correlation between P_T^W and y_W were investigated for Run Ia and were estimated to be 20 MeV in M_W . There have been an improved theoretical calculation of W and Z production, which may allow to reduce this uncertainty further.

QED Radiative corrections : Radiative corrections in M_W are rather large: the shifts in M_W due to the final state radiation are 65 MeV in the $W \rightarrow e\nu$ channel and 168 MeV in the $W \rightarrow \mu\nu$ channel. For Run Ia, the uncertainty in these shifts due to missing diagrams was estimated to be 20 MeV. Recently, a more thorough calculation [10] of radiative W and Z boson production and decay, including initial and final state radiation, finite lepton masses, and finite W , Z width effects. This will make it possible to reduce the error associated with radiative corrections substantially in the future.

- **Backgrounds**

The uncertainty which does not scale with statistics will be from the $Z \rightarrow \mu\mu$ background (one muon in the central muon chambers and the other muon in high η region) in the $W \rightarrow \mu\nu$ sample. The uncertainty due to the choice of PDF's for this background led to 10 MeV uncertainty in M_W for Run Ia. For Run II, the tracking upgrade (well measured IFT+SVX II tracks in the region $1 < |\eta| < 2$) and the forward muon upgrade (muons in the region $1.5 < |\eta| < 3$) together with the muon signature in the plug upgrade calorimeter will remove most of this background and will reduce the uncertainty.

- **Trigger Bias**

For Run Ia, there was 25 MeV uncertainty due to a possible momentum dependence of the muon triggers in the $W \rightarrow \mu\nu$ channel. For Run Ib, E_T threshold for Level-2 electrons was raised and the track resolution was degraded with luminosity. This may have caused trigger biases in both e and μ samples, which can be included in the simulation. Even though these biases are in the simulation, the uncertainty does not necessarily scale with statistics. For Run II, it is important to have unbiased triggers. That is, the momentum thresholds are low enough not to introduce a P_T or E_T dependence above 25 GeV. Also it is essential to keep triggers without any isolation requirement.

We make a conservative estimate that 2 fb^{-1} will allow CDF II to measure the W mass to $\pm 40 \text{ MeV}/c^2$, which is comparable to the overall LEP2 expectation ($\sim 40 \text{ MeV}$). The list of uncertainties is shown in

Table 2.7. In making this estimate, we have not included important beneficial effects of the muon upgrades, such as the increase in the central muon acceptance and the improved forward muon acceptance to reduce the uncertainty in the $Z \rightarrow \mu\mu$ background.

2.3.4 W Width

The leptonic branching ratio of the W may be inferred from the ratio $R = \sigma \cdot Br(W \rightarrow l\nu) / \sigma \cdot Br(Z \rightarrow ll)$, using LEP measurements for the Z couplings and a theoretical prediction of the production cross section ratio. Before the top quark was discovered, this measurement was used to exclude hidden top scenarios. Now it is a standard model consistency check. For Run Ia [11] CDF measured $Br(W \rightarrow e\nu) = 0.109 \pm 0.005$. If one further assumes standard couplings for $W \rightarrow e\nu$, one can derive a value for the total width of the W , $\Gamma_W = 2.064 \pm 0.085 \text{ GeV}$. The theoretical uncertainty in the cross section ratio is expected to limit precision to about $\pm 1\%$. However, the upgraded momentum measurement in the region $1 < |\eta| < 2$ should give improved acceptance systematics, lessening the dependence on the parton distribution functions.

For Run Ia, CDF measured $\sigma \cdot Br(W \rightarrow e\nu) = 2.51 \pm 0.12 \text{ nb}$ and $\sigma \cdot Br(Z \rightarrow ee) = 0.231 \pm 0.012 \text{ nb}$ [13]. These measurements are approaching the $\pm 3.6\%$ level of the luminosity normalization [14].

The W width can be measured directly from the shape of the transverse mass distribution (see Figure 2.17). For $M_T^W > 110 \text{ GeV}/c^2$ resolution effects are under control and using Run Ia in the mode $W \rightarrow e\nu$, CDF measured $\Gamma_W = 2.11 \pm 0.32 \text{ GeV}$ [15]. The uncertainties will likely scale with statistics allowing a $\pm 30 \text{ MeV}$ measurement for 2 fb^{-1} , much better than the LEP2 expectation of $\pm 200 \text{ MeV}$. Figure 2.18 summarizes indirect and direct measurements of Γ_W so far and the predicted uncertainty for 2 fb^{-1} from the direct measurement.

2.3.5 Gauge Boson Couplings

The Standard Model makes specific predictions for the trilinear couplings of the gauge bosons, W , Z , and γ . The nature of these couplings can be investigated via studies of $W\gamma$ and $Z\gamma$ production [16] and WW , WZ and ZZ pair production [17]. The major goals of these studies will be testing the Standard Model prediction(s) and searching for new physics. The numbers of candidates and backgrounds, and

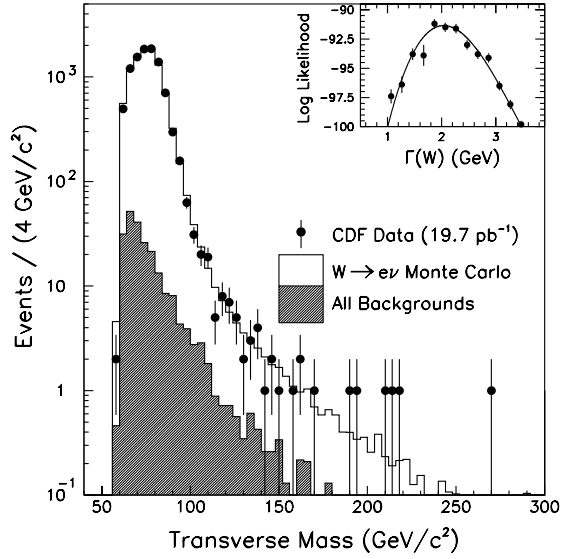


Figure 2.17: Transverse mass distribution (M_T^W) for $W \rightarrow e\nu$ candidates along with background and signal expectation. The inset is the fit to $M_T^W > 110 \text{ GeV}/c^2$.

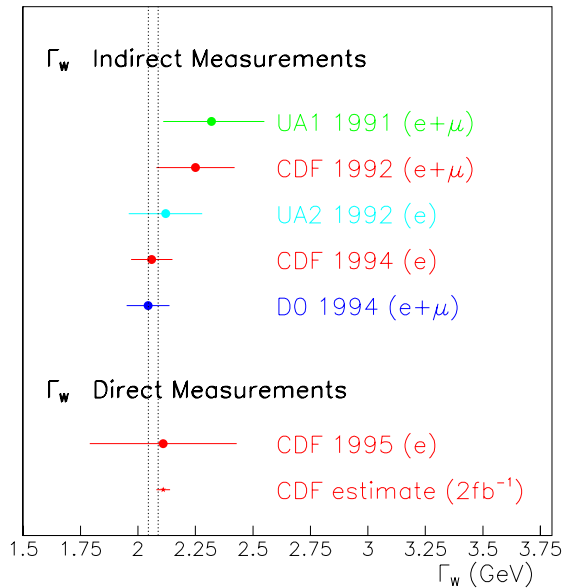


Figure 2.18: Indirect and direct measurements of Γ_W and the predicted uncertainty from the direct measurement for 2 fb^{-1} of data. The dotted band represents the standard model prediction.

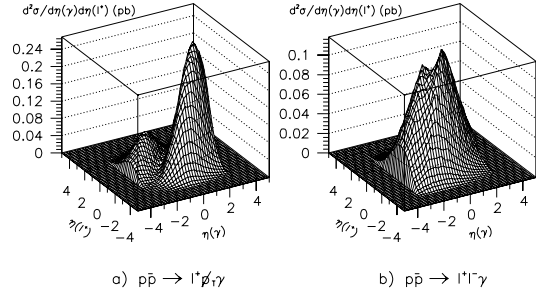


Figure 3

Figure 2.19: The double differential distribution $d^2/dy(\gamma)dy(\ell)$ for $p\bar{p} \rightarrow W^+\gamma \rightarrow \ell\nu\gamma$ (Left) and $Z\gamma \rightarrow \ell\ell\gamma$ (Right).

Diboson cross sections from CDF (preliminary)

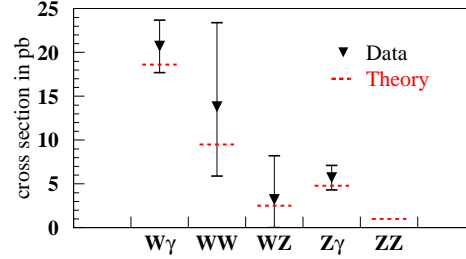


Figure 2.20: The measured cross sections of diboson productions and the theoretical predictions

the measured cross section for each production mode are summarized and the cross section is compared with the theoretical expectation in Table 2.8 and Figure 2.8.

From the absence of an excess of events at large E_T^γ in $W\gamma$ and $Z\gamma$ production, with 67 pb^{-1} combined $e + \mu$ Run Ia+Ib data we have extracted 95% CL limits on $WW\gamma$ and $ZZ\gamma$ anomalous couplings, such as $-1.8 < \Delta\kappa_\gamma < 2.0$ and $-0.7 < \lambda < 0.6$.

$W\gamma$ production in $p\bar{p}$ collisions is of special interest due to the SM prediction of a radiation amplitude zero in the charge-signed $Q_W \cdot \cos\theta_\gamma^*$ distribution at ~ -0.3 . The radiation zero is also predicted to manifest itself as a “channel” in the charge-signed $Q_W\eta_\ell$ vs. $Q_W\eta_\gamma$ 2-dimensional distribution [18] shown in Figure 2.19, and as a strong “dip” in the charge-signed photon- W decay lepton rapidity difference distribution, $Q_W \cdot (\eta_\gamma - \eta_\ell)$ at ~ -0.3 . For Run II data

Mode ($\ell = e, \mu$)	L (pb^{-1})	Data (events)	Backgrounds (events)	$\sigma_{exp}^{\text{diboson}}$ (pb)	$\sigma_{theory}^{\text{diboson}}$ (pb)
$W\gamma \rightarrow \ell\nu, \gamma$	67	109	26.4 ± 3.6	20.7 ± 3.0	18.6
$WW \rightarrow \ell\nu, \ell\nu$	110	5	1.21 ± 0.30	$10.2^{+6.5}_{-5.3}$	9.5
$WZ \rightarrow \ell\nu, \ell\ell$	110	1	$0.3^{+0.8}_{-0.3}$	$3.2^{+5.0}_{-3.2}$	2.5
$Z\gamma \rightarrow \ell\ell, \gamma$	67	31	1.4 ± 0.4	5.7 ± 1.4	4.8
$ZZ \rightarrow \ell\ell, \ell\ell$	120	1	?	?	1.0

Table 2.8: The numbers of candidates and backgrounds, and the integrated luminosity for each production mode. Also the measured cross sections and the theoretical expectations are listed.

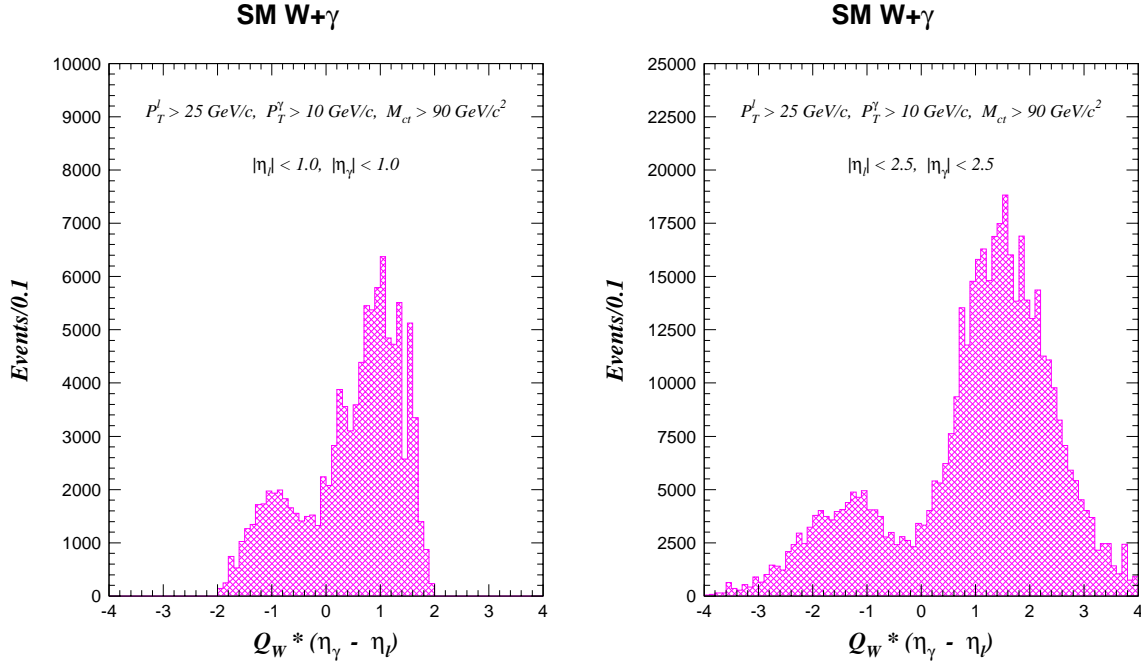


Figure 2.21: The lepton charge signed pseudo-rapidity difference distribution in the $W\gamma$ production for $|\eta_\ell| < 1.0$ and $|\eta_\gamma| < 1.0$ (Left), and $|\eta_\ell| < 2.5$ and $|\eta_\gamma| < 2.5$ (Right).

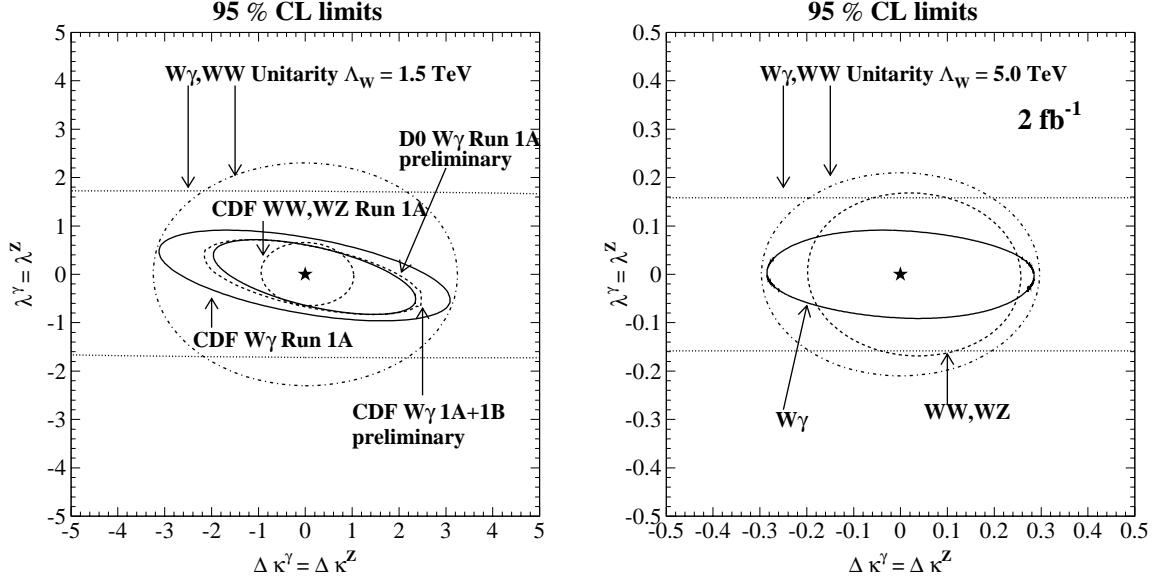


Figure 2.22: 95% CL limits on anomalous couplings. Present limits (Left) and expected limits with 2 fb^{-1} (Right) on WWV ($V = W, \gamma$) anomalous couplings.

sets the rapidity difference distribution is a more useful variable. A sufficient rapidity coverage is essential to observe the radiation zero, which is demonstrated in Figure 2.21. If both central and plug ($|\eta| < 2.5$) electrons and photons can be used, the simulations indicate that with integrated luminosities of 1 fb^{-1} it will be possible to conclusively establish the dip in the photon lepton rapidity difference distribution. On the other hand, for central electrons and photons only, the dip is not statistically significant.

Currently, we are in the process of analyzing our Run Ib data, and have succeeded in extending our photon selection into the plug region. We are also in the process of re-analyzing our Run Ia data with the new plug photon selection. From 110 pb^{-1} combined Run Ia+Ib $e + \mu$ data, including plug photons, we have increased our $W\gamma, Z\gamma$ data sample sizes by more than a factor of 10 over the original Run Ia $W\gamma, Z\gamma$ analysis. We hope to have preliminary results on (significantly) improved limits on $WW\gamma$ and $ZZ\gamma$ anomalous couplings, the $W\gamma$ radiation zero and other interesting results from analysis of the full Run Ia+Ib $e + \mu$ combined $W\gamma, Z\gamma$ data in the very near future.

For Run II, we anticipate that the current results from CDF will undergo further significant improve-

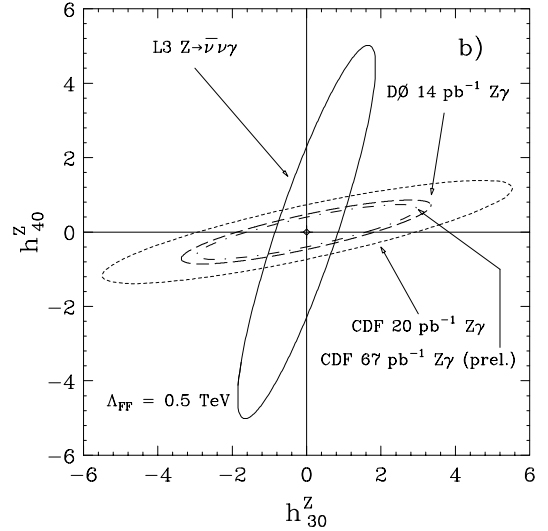


Figure 2.23: Present limits on $ZZ\gamma$ anomalous couplings.

ment(s) with 2 fb^{-1} integrated luminosity, in conjunction with the Run II upgrades of the overall tracking, calorimeter, muon and DAQ systems. Run II SM $W\gamma$ and $Z\gamma$ event yields are expected to be ~ 1500 and 450 , respectively, using the current event selection criteria.

Limits on $WW\gamma$ and WWZ anomalous couplings are also obtained from the absence of an excess of high- P_T WW and WZ boson pairs [17]. In this analysis, one vector boson is observed to decay leptonically and the other hadronically, as a jet pair of appropriate mass. The boson P_T is required to be high enough to avoid $W + \text{jets}$ background. Analysis of the Run Ia+Ib $WW, WZ \rightarrow \ell\nu + 2 \text{ jets}$ data result in the limits $-0.7 < \Delta\kappa_V < 0.9$ and $-0.5 < \lambda_V < 0.5$ at 95% CL. The absence of an excess of high- P_T WW pair events in our data also simultaneously excludes a zero-strength WWZ coupling at greater than 99% CL, thus beautifully confirming the *existence* of the delicate γWW - ZWW gauge cancellation predicted by the Standard Model, which is required if the theory is to be renormalizable!

Figure 2.22 (Left) summarizes current limits on WWV ($V = \gamma, Z$) anomalous couplings. Figure 2.23 summarizes current limits on $ZZ\gamma$ anomalous couplings. The limits on $Z\gamma\gamma$ anomalous couplings are comparable to those of $ZZ\gamma$ couplings. The sensitivity for CDF II WWV and $ZZ\gamma$ anomalous coupling measurements with 2 fb^{-1} are anticipated to be comparable, and complementary, to those anticipated from LEP-II experiments. For example, with 2 fb^{-1} of data, limits on $|\Delta\kappa_V|$ should get to about 0.3 and limits on $|\lambda_V|$ to about 0.1 (see Figure 2.22, right).

WW boson pair production, where both W 's decay leptonically can be readily distinguished from $t\bar{t}$ production and decay to dilepton final states. Using $\sim 110 \text{ pb}^{-1}$ from Run Ia+Ib data, CDF sees 5 candidates with an expected background of 1.3 events and an expected signal of 2.6 events. These events are quite central and the additional acceptance provided by the upgrades of about 30-40% comes primarily from central muon upgrades. For 2 fb^{-1} integrated luminosity, ~ 100 WW dilepton pairs are expected, for the Standard Model prediction.

2.3.6 Forward-Backward Z Asymmetry

The presence of both vector and axial-vector couplings of electroweak bosons to fermions in the pro-

cess $q\bar{q} \rightarrow Z^0/\gamma \rightarrow e^+e^-$ gives rise to an angular asymmetry, ‘‘Forward-Backward Asymmetry’’, in the emission angle of the electron in the rest frame of the electron-positron pair. This asymmetry, A_{FB} , is a direct probe of the relative strengths of the vector and axial-vector couplings over the range of Q^2 being considered. In addition, A_{FB} constrains the properties of any hypothetical heavy neutral gauge bosons not included in the Standard Model. For values of Q^2 significantly larger than M_Z^2 , A_{FB} is predicted to be large and positive (approximately 0.5), so a statistically significant measurement can be made with a small number of events.

From $\sim 110 \text{ pb}^{-1}$ of the Run I dielectron data, CDF has measured A_{FB} to be 0.074 ± 0.017 using a sample of 5473 events in the Z pole region defined by $75 < M_{ee} < 105 \text{ GeV}$, and 0.45 ± 0.11 using a sample of 172 events in the high mass region defined by $M_{ee} > 105 \text{ GeV}$. These measurements can be compared with the Standard Model predictions of 0.052 ± 0.002 and 0.528 ± 0.009 . Table 2.9 summarizes our measured values for A_{FB} and its uncertainties in both invariant mass regions.

With 2 fb^{-1} of data from Run II, we anticipate the detection of over 100,000 electron pairs resulting from Drell-Yan processes, all with invariant masses in excess of $75 \text{ GeV}/c^2$. Such a large number of events will allow for precision measurements of the angular distributions of the electron pairs both at and above the Z^0 pole.

In the vicinity of the Z^0 pole, for electron pairs with invariant mass between $75 \text{ GeV}/c^2$ and $105 \text{ GeV}/c^2$, it will be possible to extract a precision measurement of $\sin^2 \theta_W^{eff}$ from A_{FB} . The Run I measurement of A_{FB} at the Z^0 pole [19] has a total uncertainty dominated by statistical uncertainty, with the other sources of uncertainty (from background level determination and electron pair mass resolution) expected to scale with statistics as well. For instance, the Run II upgraded plug detector and tracking system expanded to higher eta region will reduce the background. The uncertainty in $\sin^2 \theta_W^{eff}$ should also scale with statistics since A_{FB} is proportional to $(\sin^2 \theta_W^{eff} - 0.25)$. Under the assumption that all uncertainties scale with statistics, we expect an uncertainty in A_{FB} of 0.003 and an uncertainty in $\sin^2 \theta_W^{eff}$ of 0.001. The Run II measurement of A_{FB} at the Z^0 pole is not expected to discriminate between different choices of parton distribution functions, as the current theoretical uncertainty in A_{FB} due to struc-

	$75 \text{ GeV}/c^2 < M_{ee} < 105 \text{ GeV}/c^2$		$M_{ee} > 105 \text{ GeV}/c^2$	
	CC	CP	CC	CP
Raw event sample	2611	2862	91	81
Background	6 ± 2	139 ± 26	1_{-1}^{+2}	27 ± 15
Predicted Asymmetry	0.048		0.52	
Measured Asymmetry	0.074		0.45	
Uncertainty in A_{FB}				
Statistical	0.016		0.10	
Background subtraction	0.003		0.05	
Mass Deconvolution	0.003		0.04	
Total uncertainty	0.017		0.11	

Table 2.9: Run I (110 pb^{-1}) measurements of A_{FB} .

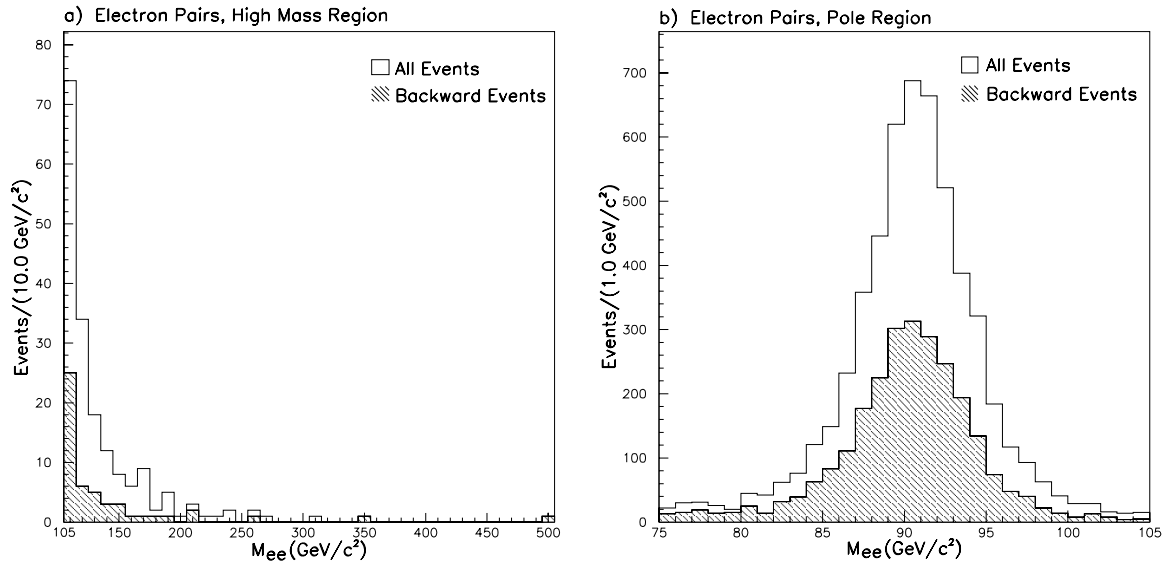


Figure 2.24: The invariant mass distribution of events in the high mass sample.(Left) and the pole region sample (Right).

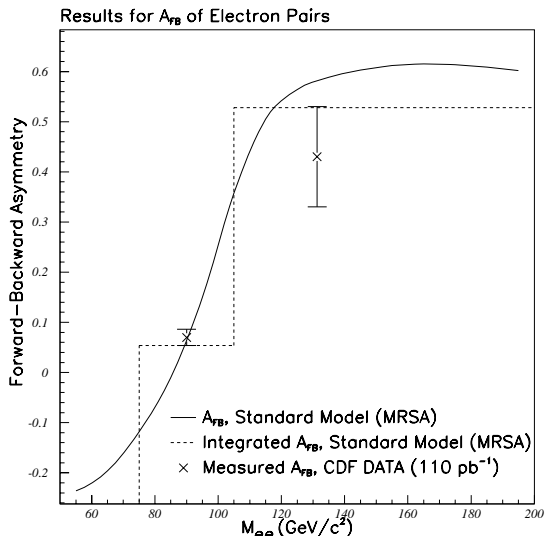


Figure 2.25: Results of our measurement of A_{FB} , compared with a Standard Model calculation. The solid line is a bin-by-bin calculation of A_{FB} (MRSA), and the dashed line is the same calculation integrated over the two mass regions.

ture function uncertainty is approximately 0.001 [20]. With the increased statistics it may also be possible to observe the rapid variation of A_{FB} as the electron pair mass varies between 75 GeV/c^2 and 105 GeV/c^2 .

It should be noted that if $\sin^2 \theta_W^{eff}$ is measured to within 0.001 as expected, then the CDF II result will be competitive with the LEP I and SLD results which measure $\sin^2 \theta_W^{eff}$ from jet charge asymmetries in hadronic Z^0 decays. For example, the ALEPH collaboration reports a measurement of $\sin^2 \theta_W^{eff}$ from light quark jets of $0.23222 \pm 0.00081(\text{stat.}) \pm 0.00070(\text{syst.}) \pm 0.00080(\text{theor.})$, where the last two sources of uncertainty arise chiefly from mismeasurement of jet charge and theoretical assumptions about jet fragmentation, respectively [21]. By virtue of measuring the inverse process, where electrons are in the final state and quarks are in the initial state, the CDF II measurement will not be sensitive to these systematic effects, and may therefore have a comparable total uncertainty with very different systematic uncertainties.

Well above the Z^0 pole, for electron pairs with invariant mass in excess of 105 GeV/c^2 , A_{FB} is dominated by Z^0/γ interference, and a large positive value is predicted for A_{FB} with a very flat dependence in

electron pair invariant mass. There can be strong variations in A_{FB} with invariant mass due to a variety of exotic physics at higher invariant mass scales, including most Z' or composite Z models [22], and also lepton compositeness models. Moreover, if a Z' is discovered at CDF II, A_{FB} measurements will provide discrimination between various Z' models [22].

As with the measurements of A_{FB} at the Z^0 pole, we expect the uncertainty in the measurements above the Z^0 pole to scale with statistics compared to the Run I measurement [19]. For electron pairs with invariant mass between 105 GeV/c^2 and 195 GeV/c^2 , we expect to collect approximately 2500-3000 events. Using this entire sample we expect to measure A_{FB} to within 0.02, and it will be possible to explore the variation of A_{FB} with invariant mass in some detail. For electron pairs with invariant mass above 195 GeV/c^2 (above the LEP 200 maximum \sqrt{s}), we expect to collect approximately 200-300 events, which should allow a measurement of A_{FB} to within 0.07. We note that these measurements neither discriminate between nor depend significantly upon the choice of proton structure function, since the theoretical uncertainty of A_{FB} in this invariant mass range due to choice of structure function is approximately 0.009 [20].

2.3.7 PDF Measurements and Issues

2.3.7.1 W Charge Asymmetry

The Run Ia CDF measurement of the W asymmetry shown in Figure 2.26 (Left) [23] is an important constraint on parton distribution functions for collider experiments, and has been used as input by both the MRS and CTEQ groups. Note that the sensitivity to the PDF's increases with lepton eta. The Ia measurement ends at $|\eta| \sim 1.8$ because the CTC track finding efficiency (see Figure 2.10) falls rapidly beyond $|\eta| \sim 1.2$ and becomes almost 0 at $|\eta| \sim 1.8$.

A new technique for extending the asymmetry measurement using electrons at higher $|\eta|$ has recently been developed by CDF for the Run Ib measurements. Here, the plug calorimeter is used to determine the energy and the shower centroid location of the electron, and the SVX is used to determine the track. No central tracking is required. A comparison of the extrapolated SVX track with the shower centroid in the calorimeter is used to determine the charge of the electron. With this technique the electron η coverage is extended up to 2.3. Due to the

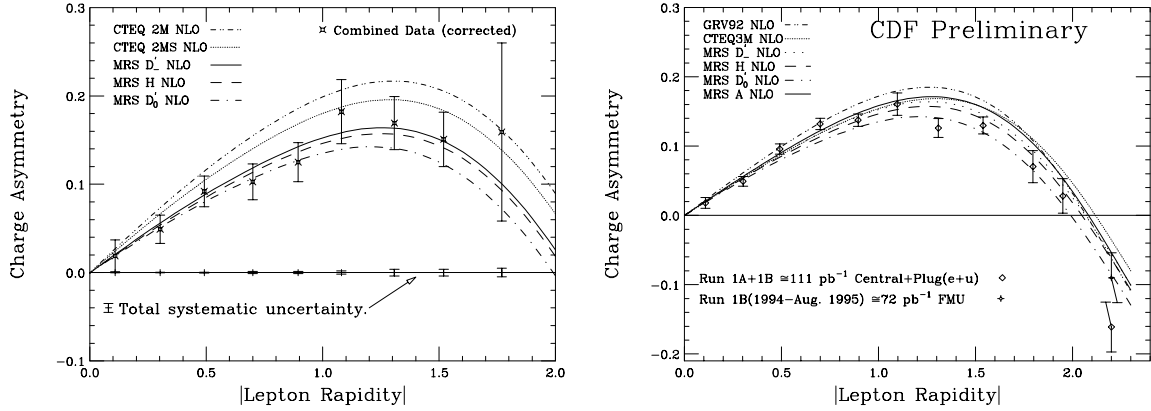


Figure 2.26: Left: Combined Run Ia W charge asymmetry measurement using muons and central and plug electrons. These data have been used as input in determining recent PDF sets. Right: Combined W charge asymmetry using Run Ia and Ib data including the forward muons.

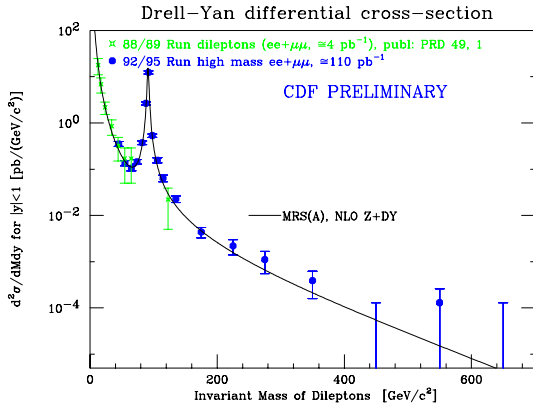


Figure 2.27: Drell-Yan dilepton (e^+e^- , $\mu^+\mu^-$) production cross section from Run Ia and Ib as a function of the dilepton invariant mass.

short length of the SVX', the SVX tracking finding efficiency is only 50–60% as shown in see Figure 2.10. For Run Ib, we have also measured the W charge asymmetry in $2 < |\eta^\mu| < 2.5$ using the current forward muon detector. All of these measurements from central electrons, plug electrons, central muons, and forward muons are combined and are shown in Figure 2.26 (Right).

The data in the central region probes the d and u distributions in the x region between 0.02 and 0.15. The forward data probes the region between 0.006 (a new region of x) and 0.35. These forward data indicate that further tuning of the d and u distributions

in the current PDF's might be needed.

The new Run II plug electromagnetic calorimeter and shower max detectors offer greater improvement over the present plug. In addition, the tracking with SVX II and IFT will be much better. These new detectors can be used to further extend the W asymmetry electron data in the forward directions. The tracking upgrade and the muon toroid move will allow the extension of the asymmetry measurement using muons to higher $|\eta|$ as well. The measurements should remain statistically dominated through 2 fb^{-1} .

2.3.7.2 Drell-Yan production

Cross section measurements of Drell-Yan production [24] (especially the low mass region) can be used to get further constraints on PDFs. The Run Ia+Ib Drell-Yan cross section measurements using central electrons are shown in Figure 2.27. The low mass Drell-Yan data and forward data are currently under analysis. The main difficulties in these area are estimating QCD backgrounds. The new technique described in previous paragraphs now provides the ability to determine the charge of an electron in the forward direction, and allows a direct measurement of the QCD background by a comparison of like-sign to opposite-sign events. Therefore, the Drell-Yan measurement can now be extended to the forward direction (for both electron and muon pairs), and the low mass region. The low mass data is sensitive to the very low x region which has never been explored be-

fore at the Tevatron. Run II upgrades to the DAQ bandwidth will be important for this program in order to preserve our ability to trigger on low p_T lepton pairs.

The y distributions of Drell-Yan dilepton pairs can be measured as a function of the dilepton invariant mass. These distributions will also contain the information of PDF's.

The high mass Drell Yan data from Run IA and IB, on the other hand, can now be used to place limits on compositeness around the 3 TeV range. These limits can be greatly improved in Run II.

Bibliography

- [1] S. L. Glashow, Nucl. Phys. **22**, 579 (1961); S. Weinberg, Phys. Rev. Lett. **19**, 1264 (1967); A. Salam, in *Elementary Particle Theory: Relativistic Groups and Analyticity*, ed. N. Svartholm (Almqvist and Wiksell, Stockholm, 1968), p. 367.
- [2] F. S. Merritt, H. Montgomery, A. Sirlin and M. Swartz, DPF report on Precision Tests of Electroweak Physics, CDF Note 3154.
- [3] F. Abe *et al.* (CDF Collaboration), Phys. Rev. Lett. **74**, 2626 (1995), S. Abachi *et al.* (D0 Collaboration), Phys. Rev. Lett. **74**, 2632 (1995).
- [4] H. Aihara, *et al.*, “Anomalous Gauge Boson Interactions”, Summary of the Subgroup on Anomalous Gauge Boson Interactions of the DPF Long-Range Planning Study, in “Electroweak Symmetry Breaking and Beyond the Standard Model, edited by T. Barklow, S. Dawson, H. Haber and J. Siegrist, World Scientific, Singapore (1995).
- [5] H. Aihara, *et al.*, “Intermediate Vector Boson Physics”, Summary of the TeV-2000 Working Subgroup on Electroweak Physics, edited by R. Brock and D. Amidei, Fermilab, (1996).
- [6] D. Schaile, presented at 10th International Workshop on $p\bar{p}$ Interactions, Fermilab 1995.
- [7] F. Abe *et al.*(CDF), Phys. Rev. **D43**, 2070 (1991).
- [8] F. Abe *et al.*(CDF), Accepted for publication in Phys. Rev., FERMILAB-PUB-95/033-E.
- [9] The curves are calculated using a FORTRAN program from F. Halzen and B.A. Kniehl (private communication), described in Nucl. Phys. **B353**, 567 (1990). See Ref. 4 for details.
- [10] U. Baur and D. Zeppenfeld, Phys. Rev. Lett. **75**, 1002 (1995).
- [11] F. Abe *et al.*(CDF), Phys. Rev. Lett. **73**, 220 (1994).
- [12] Particle Data Group, Phys. Rev. **D50**, p 1173 (1994).
- [13] W. Badgett (CDF), proc. DPF Abaquerque (1994), FERMILAB-CONF-95/258-E.
- [14] F. Abe *et al.*(CDF), Phys. Rev. **D50**, 5550 (1994).
- [15] F. Abe *et al.*(CDF), Phys. Rev. Lett. **74**, 341 (1995).
- [16] F. Abe, *et al.*, The CDF Collaboration, “Measurement of W -Photon Couplings in $p\bar{p}$ Collisions at $\sqrt{s} = 1.8$ TeV”, Phys. Rev. Lett. **74**, 1936 (1995); F. Abe, *et al.*, The CDF Collaboration, “Limits on Z -Photon Couplings from $p\bar{p}$ Interactions at $\sqrt{s} = 1.8$ TeV”, Phys. Rev. Lett. **74**, 1941 (1995).
- [17] F. Abe, *et al.*, The CDF Collaboration, “Limits on WWZ and $WW\gamma$ Couplings from WW and WZ Production in $p\bar{p}$ Interactions at $\sqrt{s} = 1.8$ TeV”, Phys. Rev. Lett. **75**, 1017 (1995).
- [18] U. Baur, S. Errede and G. Landsberg, “Rapidity Correlations in $W\gamma$ Production at Hadron Colliders”, Phys. Rev. **D50**, 1917 (1994).
- [19] F. Abe *et al.*, Fermilab Report No. FERMILAB-PUB-96/071-E.
- [20] U. Baur (private communication).
- [21] ALEPH Collaboration, D. Buskulic *et al.*, CERN-PPE/96-09.
- [22] J. L. Rosner, Fermilab Report No. FERMILAB-PUB-95/394-T.
- [23] F. Abe *et al.*(CDF), Phys. Rev. Lett. **74**, 850 (1995).
- [24] F. Abe *et al.*(CDF), Phys. Rev. **D49**, R1 (1994).